AUTOMATICALLY INFERRING DATA QUALITY FOR SPATIOTEMPORAL FORECASTING

Sungyong Seo
Department of Computer Science
University of Southern California
sungyons@usc.edu

Arash Mohegh, George Ban-Weiss
Dept of Civil and Environmental Engineering
University of Southern California
{mohegh,banweiss}@usc.edu

Yan Liu
Department of Computer Science
University of Southern California
yanliu.cs@usc.edu

ABSTRACT

The importance of learning from spatiotemporal data has been growing with increasing amounts of data sources distributed over space. While numerous studies have been done for analyzing spatiotemporal signals, existing models have assumed that heterogeneous data sources in the spatial domain are equally reliable over time. In this paper, we propose a novel method that estimates time-varying data quality levels based on local variations of spatiotemporal signals without explicit labels that designate data quality. Furthermore, we integrate our estimate of data quality level with graph convolutional networks to exploit their efficient structure, because spatially distributed data sources form natural graphs. Finally, we evaluate the proposed method by simulating a forecasting task with real-world climate data.

1 INTRODUCTION

Recent advances with GPS-equipped technology have facilitated the collection of large spatiotemporal datasets. As the amount of spatiotemporal data increases, many have proposed representing this data as time-varying graph signals in various domains, such as sensor networks (Shi et al., 2015; Zhu & Rabbat, 2012), climate analysis (Chen et al., 2014; Mei & Moura, 2015), traffic control systems (Li et al., 2017; Yu et al., 2017), and biology (Mutlu et al., 2012; Yu et al., 2015).

While many works have been proposed to exploit both *spatial structures* and *temporal signals*, most models have implicitly assumed that each signal source node in a spatial structure is equally reliable over time, without considering the data quality of different sources. However, a large amount of data comes from heterogeneous sources that have different levels of noise (Song et al., 2015; Zhang & Chaudhuri, 2015). Moreover, the noises of each source can *vary over time* due to abrupt malfunctions of sensors. Such noises can be considered as small data perturbations, which are also known to be capable of deceiving deep neural networks and cause undesired behaviors (Goodfellow et al., 2014; Koh & Liang, 2017). Thus, it is naturally desired to differentiate the data quality level of each source. An important technical problem arises when developing an estimate of data quality level. How can such data quality for many different sources be estimated without labels, which are laborious and expensive to obtain? By answering this question, we can develop a practical model that automatically differentiates between high and low quality sources.

In this paper, we consider a learning problem of spatiotemporal signals that are represented by time-varying graph signals for different data qualities. Given a graph $\mathcal{G} = (\mathcal{V}, \mathcal{E}, \mathbf{W})$ and observations $\mathcal{X} \in \mathbb{R}^{N \times M \times T}$ where N, M, T are the number of vertices, the types of signals, and the length of time-varying signals, respectively, we propose a model that is able to exploit structural information (spatial features) as well as temporal behaviors (time series). On top of the time-varying graph signals, we implement graph-based neural networks that encode the level of data quality at each vertex into a scalar by looking at neighboring signals observed at a set of K-hop neighboring vertices.

There are multiple definitions of data quality but high quality data is generally considered as it is fit for intended uses in operations, decision making and planning (Redman, 2008). Here, we narrow down the definition of the term as *a penalizing quantity for high local variations*.

The contributions of our paper are the following. First, we define the concept of a data quality level at each vertex in a graph using a *local variation* of the vertex. The local variation at each vertex depends on the local spatial structure and neighboring signals. We propose a function of the local variation at the vertex to infer the data quality level in an unsupervised manner without any explicitly given quality labels. It is worth to note that it is flexible to define the data quality function depending on tasks and characteristics of datasets. Secondly, we combine the quality level with an objective function defined by the task at hand. Specifically, the quality level is used as a regularizer constant in the objective function. Finally, we demonstrate that the data quality is an essential factor which can improve the predictive performance of common tasks, such as time-series forecasting, on real-world climate datasets.

Related work The first set of work related to our study is about learning and processing graph signals or features. Spectral graph theory (Chung, 1997; Von Luxburg, 2007; Shi et al., 2015) has been developed as a main study to understand two aspects of graph signals: structures and signals. Under this theory many works have been introduced to exploit convolutional neural networks (CNNs) which provide an efficient architecture to extract localized patterns from regular grids, such as images (Krizhevsky et al., 2012). Bruna et al. (2014) introduce how to learn convolutional parameters based on the spectrum of the graph Laplacian. Later, Henaff et al. (2015) extend the spectral aspect of CNNs on graphs into large-scale learning problems. From the pioneer works about graph convolutional networks (GCN), Defferrard et al. (2016) propose a spectral formulation for fast localized filtering with efficient pooling. Furthermore, Kipf & Welling (2017) re-formularize existing ideas into layer-wise neural networks that can be tuned through backpropagation rule with a first-order approximation of spectral filters introduced in Hammond et al. (2011). On top of these studies, we propose a graph convolutional layer that maps spatiotemporal features into a data quality level.

There are a number of works about considering data qualities and handling heterogeneous data sources. Urner et al. (2012) is the first theoretical work that proposes a mixture of two types of labels for supervised learning. One type of the labels is considered as high quality labels from an expensive source (domain experts) while another type is from error-prone crowdsourcing. Since the reliability or quality of the labels is different, it is not desired to consider them equally. They propose a learning algorithm that is able to utilize the error-prone labels to reduce the cost required for the expert labeling. Zhang & Chaudhuri (2015) address issues from strong and weak labelers by developing an active learning algorithm minimizing the number of label requests. Song et al. (2015) focus on the data of variable quality resulting from heterogeneous sources. They define the concept of heterogeneity of data and develop a method of adjusting the learning rate based on the heterogeneity. Unlike these existing works, we provide a method to differentiate heterogeneous sources based on neighborhood signals without any explicit labels.

Outline We review graph signal processing to define the local variation and a data quality level (DQL) with graph convolutional networks in Section 2. In Section 3, we provide how the data quality levels are exploited with recurrent neural networks to differentiate reliability of observations on vertices. Also, we construct a forecasting model, DQ-LSTM. Our main result is presented in Section 4 with other baselines. In Section 5 we discuss its properties and interpret the data reliability inferred from our model. We then conclude with Section 6.

2 PRELIMINARIES

We first show how to define the local variation at a vertex based on graph signals. Then, we explain how the variational features at each vertex can be used to generate a data quality level.

2.1 LOCAL VARIATION

We focus on the graph signals defined on an undirected, weighted graph $\mathcal{G} = (\mathcal{V}, \mathcal{E}, \mathbf{W})$, where $\mathcal{V}$ is a set of vertices with $|\mathcal{V}| = N$ and $\mathcal{E}$ is a set of edges. $\mathbf{W} \in \mathbb{R}^{N \times N}$ is a random-walk normalized weighted adjacency matrix which provides how two vertices are relatively close. When the elements

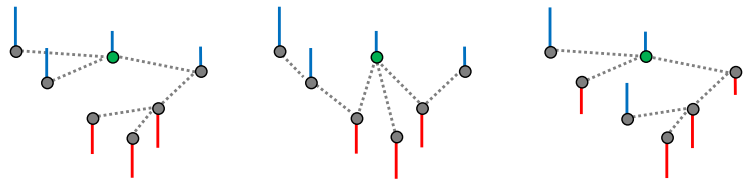

(a) Original graph (b) Different adjacency (c) Different graph signal

Figure 1: Each bar represents the signal value at the vertex where the bar originates. Blue and red color indicate positive and negative values, respectively. Local variations at the green node are (a) 1.67 (b) 25 and (c) 15, respectively.

W_{ij} are not be expliticly provided by dataset, the graph connectivity can be constructed by various distance metrics, such as Euclidean distance, cosine similarity, and a Gaussian kernel (Belkin & Niyogi, 2002), on the vertex features $\mathbf{V} \in \mathbb{R}^{N \times F}$ where F is the number of the features.

Once all the structural connectivity is provided, the local variation can be defined by the edge derivative of a given graph signal $\mathbf{x} \in \mathbb{R}^N$ defined on every vertex (Zhou & Schölkopf, 2004).

$$\left.\frac{\partial \mathbf{x}}{\partial e}\right|_{e=(i,j)} = \sqrt{W_{ij}}(x(j) - x(i)), \tag{1}$$

where $e = (i, j)$ is defined as a direction of the derivative and $x(i)$ is a signal value on the vertex i. The graph gradient of $\mathbf{x}$ at vertex i can be defined by Eq. 1 over all edges joining the vertex i.

$$\nabla_i \mathbf{x} = \left(\left.\frac{\partial \mathbf{x}}{\partial e}\right|_{e=(i,j)} \middle| \, j \in \mathcal{N}_i \right), \tag{2}$$

where $\mathcal{N}_i$ is a set of neighbor vertices of the vertex i. While the dimesion of the graph gradient is different due to the different number of neighbors of each vertex, the local variation at vertex i can be defined by a norm of the graph gradient:

$$\|\nabla_i \mathbf{x}\|_2^2 = \sum_{j \in \mathcal{N}_i} W_{ij}(x(j) - x(i))^2, \tag{3}$$

Eq. 3 provides a measure of local variation of $\mathbf{x}$ at vertex i. As it indicates, if all neighboring signals of i are close to the signal at i, the local variation at i should be small and it means *less fluctuated signals* around the vertex. As Eq. 3 shows, the local variation is a function of a structural connectivity $\mathbf{W}$ and graph signals $\mathbf{x}$. Figure 1 illustrates how the two factors affect the local variation at the same vertex.

The concept of the local variation is easily generalized to multivariate graph signals of M different measures by repeatedly computing Eq. 3 over all measures.

$$\mathbf{L}_i = (\|\nabla_i \mathbf{x}^1\|_2^2, \cdots, \|\nabla_i \mathbf{x}^m\|_2^2, \cdots, \|\nabla_i \mathbf{x}^M\|_2^2), \tag{4}$$

where $\mathbf{x}^m \in \mathbb{R}^N$ corresponds the mth signals from multiple sensors. As Eq. 4 indicates, $\mathbf{L}_i$ is a M dimensional vector describing local variations at the vertex i with respect to the M different measures.

Finally, it is desired to represent Eq. 4 in a matrix form to be combined with graph convolutional networks later.

$$\mathbf{L}(\mathbf{W}, \mathbf{X}) = (\mathbf{D} + \mathbf{W})(\mathbf{X} \odot \mathbf{X}) - 2(\mathbf{X} \odot \mathbf{W}\mathbf{X}), \tag{5}$$

where $\mathbf{D}$ is a degree matrix defined as $D_{ii} = \sum_j W_{ij}$ and $\odot$ is an element-wise product operator. $\mathbf{X}$ is a $N \times M$ matrix describing multivariate graph signals on N vertices and $\mathbf{x}^m$ is a mth column of $\mathbf{X}$. $\mathbf{L} \in \mathbb{R}^{N \times M}$ is a local variation matrix and L_{im} is the local variation at the vertex i with respect to the mth signal.

2.2 DATA QUALITY LEVEL

While the term of data quality has been used in various ways, it generally means "*fitness of use*" for intended purposes (Juran & Godfrey, 1999). In this section, we will define the term under the data property we are interested in and propose how to exploit the data quality level into a general framework.

Given a multivariate graph signal $\mathbf{X} \in \mathbb{R}^{N \times M}$ on vertices represented by a feature matrix $\mathbf{V} \in \mathbb{R}^{N \times F}$, we assume that a signal value at a certain vertex i is desired not be significantly different with signals of neighboring vertices $j \in \mathcal{N}_i$. This is a valid assumption if the signal value at the vertex i is dependent on (or function of) features of the vertex i when an edge weight is defined by a distance in the feature vector space between two vertices. In other words, if two vertices have similar features, they are connected to form the graph structure and the signal values observed at the vertices are highly likely similar. There are a lot of domains which follow the assumption, for instance, geographical features (vertex features) and meteorological observations (graph signal) or sensory nervous features and received signals.

Under the assumption, we define the data quality level (score) at a vertex i as a function of local variations of i:

$$s_i = q(\mathbf{L}_i), \tag{6}$$

It is flexible to choose the function q. For example, s_i can be defined as an average of $\mathbf{L}_i$. If so, all measures are equally considered to compute the data quality at vertex i. In more general sense, we can introduce parameterized function $q(\mathbf{L}_i; \mathbf{\Phi})$ and learn the parameters through data. Kipf & Welling (2017) propose a method that learns parameters for graph-based features by the layer-wise graph convolutional networks (GCN) with arbitrary activation functions. For a single layer GCN on a graph, the latent representation of each node can be represented as:

$$\mathbf{Z} = \sigma(\hat{\mathbf{A}}\mathbf{X}\mathbf{\Theta}), \tag{7}$$

where $\hat{\mathbf{A}} = (\mathbf{D}+\mathbf{I}_N)^{-\frac{1}{2}}(\mathbf{A}+\mathbf{I}_N)(\mathbf{D}+\mathbf{I}_N)^{-\frac{1}{2}}$ provides *structural connectivities* of a graph and $\mathbf{\Theta}$ is a trainable parameter matrix. σ is an activation function. By stacking $\sigma(\hat{\mathbf{A}}\mathbf{X}\mathbf{\Theta})$, it is able to achieve larger receptive fields with multi-layer GCN. See details in Kipf & Welling (2017).

We can replace $\hat{\mathbf{A}}\mathbf{X}$ with $\mathbf{L}$ which is also a function of the weighted adjacency $\mathbf{W}$ and the graph signal $\mathbf{X}$. Note that values in row i of $\hat{\mathbf{A}}\mathbf{X}$ and $\mathbf{L}$ are a function of values at i as well as neighbors of i. Although $\mathbf{L}$ only exploits nearest neighbors (i.e., 1-hop neighbors), it is possible to consider K-hop neighbors to compute the local variations by stacking GCN before applying Eq. 3. The generalized formula for the data quality level can be represented as:

$$\mathbf{Z} = \sigma_K(\hat{\mathbf{A}}\sigma_{K-1}(\hat{\mathbf{A}} \cdots \sigma_1(\hat{\mathbf{A}}\mathbf{X}\mathbf{\Theta_1}) \cdots \mathbf{\Theta}_{K-1})\mathbf{\Theta}_K), \tag{8}$$

$$\mathbf{s} = \sigma_L(\mathbf{L}(\mathbf{W}, \mathbf{Z})\mathbf{\Phi}). \tag{9}$$

where K is the number of GCN layers and $\mathbf{s} = (s_1, s_2, \cdots, s_N)$ is the data quality level of each vertex incorporating K-hop neighbors. We propose some constraints to ensure that a higher s_i corresponds to *less fluctuated* around i. First, we constrain $\mathbf{\Phi}$ to be positive to guarantee that larger elements in $\mathbf{L}$ cause larger $\mathbf{L}\mathbf{\Phi}$ that are inputs of σ_L. Next, we use an activation function that is inversely proportional to an input, e.g., $\sigma_L(x) = \frac{1}{1+x}$, to meet the relation between the data quality s_i and the local variations $\mathbf{L}_i$. Once $\mathbf{s}$ is obtained, it will be combined with an objective function to assign a penalty for each vertex loss function.

3 MODEL

In this section, we give the details of the proposed model, which is able to exploit the data quality defined in Section 2.2 for practical tasks. First, it will be demonstrated how the data quality network DQN is combined with recurrent neural networks (LSTM) to handle time-varying signals. We, then, provide how this model is trained over all graph signals from all vertices.

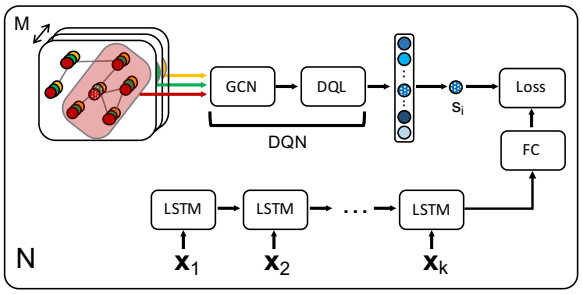

Figure 2: Architecture of DQ-LSTM that consists of GCN followed by the data quality network DQN and LSTM. GCN are able to extract localized features from given graph signals (different colors correspond to different signals) and DQN computes the data quality of each vertex. N is the number of vertices, i.e. each loss function on each vertex is weighted by the quality level s_i. Note that the dot-patterned circles denote the current vertex i.

Data quality network In Section 2.2, we find that the local variations around all vertices can be computed once graph signals $\mathbf{X}$ are given. Using the local variation matrix $\mathbf{L}$, the data quality level at each vertex s_i can be represented as a function of $\mathbf{L}_i$ with parameters $\mathbf{\Phi}$ (See Eq. 6). While the function q is not explicitly provided, we can parameterize the function and learn the parameters $\mathbf{\Phi} \in \mathbb{R}^M$ through a given dataset.

One of straightforward parameterizations is based on fully connected neural networks. Given a set of features, neural networks are efficient to find nonlinear relations among the features. Furthermore, the parameters in the neural networks can be easily learned through optimizing a loss function defined for own purpose. Thus, we use a single layer neural networks $\mathbf{\Phi}$ followed by an activation function $\sigma_L(\cdot)$ to transfer the local variations to the data quality level. Note that multi-layer GCN can be used between graph signals and DQN to extract convolved signals as well as increase the size of convolution filters. (See Eq. 8 and 9). This multi-layer neural networks are efficient to learn nonlinear interactions of K-hop nodes which are not easily learnable by graph polynomial filters in Sandryhaila & Moura (2013).

Long short term memory Recurrent neural networks (RNNs) are especially powerful to extract latent patterns in time series which has inherent dependencies between not only adjacent data points but also distant points. Among existing various RNNs, we use Long short term memory (LSTM) (Hochreiter & Schmidhuber, 1997) to handle the temporal signals on vertices for a regression task. We feed finite lengths k of sequential signals into LSTM as an input series to predict the observation at next time step. The predicted value is going to be compared to a true value and all parameters in LSTM will be updated via backpropagation through time.

DQ-LSTM Figure 2 illustrates how the data quality networks with LSTM (DQ-LSTM) consists of submodules. Time-varying graph signals on N vertices can be represented as a tensor form, $\mathcal{X} \in \mathbb{R}^{N \times M \times T}$ where the total length of signals is T. First, the time-varying graph signals for each vertex are segmentized to be fed into LSTM. For example, $\mathcal{X}(i, :, h : h + k - 1)$ is one of segmentized signals on vertex i starting at $t = h$. Second, the graph signals for all vertices at the last time stamp $\mathcal{X}(:, :, h+k-1)$ are used as an input of GCN followed by DQN. Hence, we consider the data quality level by looking at the local variations of the last signals and the estimated quality level s_i is used to assign a weight on the loss function defined on the vertex i. We use the mean squared error loss function.

For each vertex i, DQ-LSTM repeatedly reads inputs, predicts outputs, and updates parameters as many as a number of segmentized length k time series.

$$\mathcal{L}_i = \frac{1}{n_i} \sum_{j=1}^{n_i} s_i \|\hat{\mathcal{X}}(i, :, k + j - 1) - \mathcal{X}(i, :, k + j - 1)\|_2^2 + \beta \|\mathbf{\Phi}\|_2^2 \tag{10}$$

where n_i is the number of segmentized series on vertex i and $\hat{\mathcal{X}}(i, :, k + j - 1)$ is a predicted value from a fully connected layer (FC) which reduces a dimension of an output vector from LSTM. L_2

regularization is used to prevent overfitting. Then, the total loss function over all vertices is as $\mathcal{L} = \frac{1}{N}\sum_{i=1}^{N}\mathcal{L}_i$.

4 EXPERIMENTS

In this section, we evaluate DQ-LSTM on real-world climate datasets. In the main set of experiments, we evaluate the mean absolute error (MAE) of the predictions produced by DQ-LSTM over entire weather stations. In addition, we analyze the data quality levels estimated by DQ-LSTM.

4.1 DATASETS

We use real-world datasets on meteorological measurements from two commercial weather services, Weather Underground(WU) and WeatherBug(WB). Both datasets provide real-time weather information from personal weather stations. In the datasets, all stations are distributed around Los Angeles County, and geographical characteristics of each station are also provided. These characteristics would be used as a set of input features $\mathbf{V}$ to build a graph structure. The list of the static 11 characteristics is, *Latitude, Longitude, Elevation, Tree fraction, Vegetation fraction, Albedo, Distance from coast, Impervious fraction, Canopy width, Building height,* and *Canopy direction*.

Meteorological signals at each station are observed through the installed instruments. The types of the measurements are *Temperature, Pressure, Relative humidity, Solar radiation, Precipitation, Wind speed*, and *Wind direction*. Since each weather station has observed the measurements under its own frequency (e.g., every 5 minutes or every 30 minutes), we fix the temporal granularity at 1 hour and aggregate observations in each hour by averaging them. We want to ensure that the model can be verified and explained physically within one meteorological regime before applying it to the entire year with many other regimes. Since it is more challenging to predict temperatures in the summer season of Los Angeles due to the large fluctuation of daytime temperatures (summer: 36°F / 19°C and winter: 6°F / 3.3°C between inland areas and the coastal Los Angeles Basin), we use 2 months observations from each service, July/2015 and August/2015, for our experiments. The dataset description is provided in Appendix A.

4.2 GRAPH GENERATION

Since structural information between pairs of stations is not directly known, we need to construct a graph of the weather stations. In general graphs, two nodes can be interpreted as similar nodes if they are connected. Thus, as mentioned in Section 2.1, we can compute a distance between two nodes in the feature space. A naive approach to defining the distance is using only the geolocation features, *Latitude* and *Longitude*. However, it might be inappropriate because other features can be significantly different even if two stations are fairly close. For example, the distance between stations in the Elysian Park and Downtown LA is less than 2 miles, however, the territorial characteristics are significantly different. Furthermore, the different characteristics (e.g., Tree fraction or Impervious fraction) can affect weather observations (especially, temperature due to urban heat island effect). Thus, considering only physical distance may improperly approximate the meteorological similarity between two nodes.

To alleviate this issue, we assume that all static features are equally important. This is a reasonable assumption because we do not know which feature is more important since each feature can affect weather measurements. Thus, we normalize all spatial features. In this experiment, we use the Gaussian kernel $e^{(-\gamma\|V_i - V_j\|^2)}$ with $\gamma = 0.2$ and 0.6 for WU and WB, respectively, and make weights less than 0.9 zero (i.e., disconnected) such that the average number of node neighbors is around 10.

4.3 BASELINES

We compare our approach to well-studied baselines for time-series forecasting. First, we compare against a stochastic process, autoregressive (AR), which estimates future values based on past values. Second, we further compare against a simple LSTM. This model is expected to infer mixed-dependencies among the input multivariate signals and provide a reference error of the neural net-

Table 1: Forecasting mean absolute error (MAE) (°C)

	AR	LSTM	GCN-LSTM (K=1)	GCN-LSTM (K=2)	DQ-LSTM (K=0)	DQ-LSTM (K=1)
WU7	0.5342	0.5823 (0.0656)	0.5152 (0.0081)	0.5073 (0.0261)	0.5096 (0.0152)	**0.4788** (0.0111)
WU8	0.5862	0.5911 (0.0221)	0.5356 (0.0398)	0.5151 (0.0272)	0.5087 (0.0117)	**0.4856** (0.0086)
WB7	0.4812	0.4725 (0.0277)	0.4687 (0.0348)	0.4411 (0.0321)	0.4588 (0.0148)	**0.4108** (0.0129)
WB8	0.5133	0.5435 (0.0376)	0.5412 (0.0483)	0.5296 (0.0164)	0.4602 (0.0440)	**0.4574** (0.0178)

works based model. Lastly, we use graph convolutional networks (Kipf & Welling, 2017) which are also able to infer the data quality level from a given dataset. We test a single layer GCN ($K = 1$) and two-layer GCN ($K = 2$).

4.4 Experimental seting

Since DQ-LSTM and our baselines are dependent on previous observations, we set a common lag length of $k = 10$. For the deep recurrent models, the k-steps previous observations are sequentially inputted to predict next values. All deep recurrent models have the same 50 hidden units and one fully connected layer ($\mathbb{R}^{50\times 1}$) that provides the target output. For GCN-LSTM and DQ-LSTM, we evaluate with different numbers of layers (K) of GCN. We set the dimension of the first ($K = 1$) and second ($K = 2$) hidden layer of GCN as 10 and 5, respectively, based on the cross validation. The final layer always provides a set of scalars for every vertex, and we set $\beta = 0.05$ for the $L2$ regularization of the final layer. We use the Adam optimizer (Kingma & Ba, 2015) with a learning rate of 0.001 and a mean squared error objective.

We split each dataset into three subsets: training, validation, and testing sets. The first 60% observations are used for training, the next 20% is used to tune hyperparameters (validation), and the remaining 20% is used to report error results (test). Among the measurements provided, *Temperature* is used as the target measurement, i.e., output of LSTM, and previous time-step observations, including Temperature, are used as input signals. We report average scores over 20 trials of random initializations.

5 Results and Discussion

5.1 Forecasting experiment

Experimental results are summarized in Table 1. We report the temperature forecasting mean absolute error (MAE) of our DQ-LSTM model with standard deviations. Meteorological measurements for July and August are denoted by 7 and 8, and K indicates the number of GCN layers. Overall, the models that account for graph structures outperform AR and LSTM. While the node connectivities and weights are dependent on our distance function (Section 4.2), Table 1 clearly shows that knowing the neighboring signals of a given node can help predict next value of the node.

Although GCN are able to transfer a given signal of a vertex to a latent representation that is more compact and expressive, GCN have difficulty learning a mapping from neighboring signals to data quality level directly, unlike DQ-LSTM which pre-transfers the signals to local variations explicitly. In other words, given signal X, what GCN learns is $s = f(X)$ where s is the data quality we want to infer from data; however, DQ-LSTM learns $s = g(Y = h(X))$ where Y is a local variation matrix given by X in a closed form, h. Thus, lower MAEs of DQ-LSTM verify that our assumption in Section 2.2 is valid and the local variations are a useful metric to measure data quality level. It is also noteworthy that DQ-LSTM with a GCN reports the lowest MAE among all models. This is because the additional trainable parameters in GCN increase the number of neighboring nodes that are accounted for to compute better local variations.

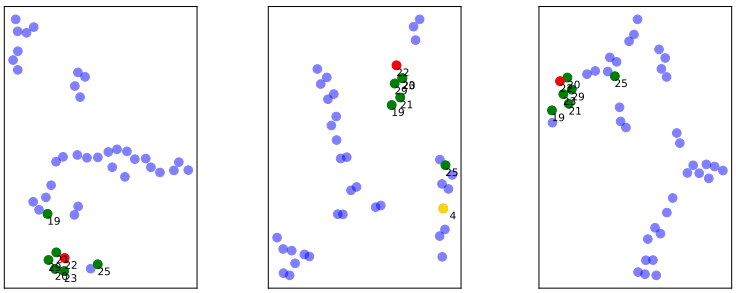

(a) $t = 0$ (b) $t = 4$ (c) $t = 8$

Figure 3: t-SNE visualization of outputs of GCN in DQ-LSTM. Red dot denotes the reference node and green dots are the adjacent nodes of the red dot. (a), (b) and (c) illustrate how the embeddings of spatiotemporal signals changes. At $t = 4$, the v_{25} node is relatively far from other green nodes because it is connected with the v_4 node which is not a neighbor of red dot. All nodes come from Weather Underground.

5.2 Node embedding and low-quality detection

As DQ-LSTM can be combined with GCN, it is possible to represent each node as an embedding obtained from an output of GCN. Embeddings from deep neural networks are especially interesting since they can capture *distances* between nodes. These distances are not explicitly provided but inherently present in data. Once the embeddings are extracted, they can be used for further tasks, such as classification and clustering (Grover & Leskovec, 2016; Kipf & Welling, 2017). Moreover, since the embeddings have low dimensional representations, it is more efficient to visualize the nodes by manifold learning methods, such as t-SNE (Maaten & Hinton, 2008). Visualization with spatiotemporal signals is especially effective to show how similarities between nodes change.

Figure 3 shows varying embedding distributions over time. The green dots are neighbors of a red dot, and they are closely distributed to form a cluster. There are two factors that affect embeddings: *temporal signals* and *spatial structure*. Ideally, connected nodes have observed similar signals and thus, they are mapped closely in the embedding space. However, if one node v_i measures a fairly different value compared to other connected values, the node's embedding will also be far from its neighbors. Furthermore, if one node v_i is connected to a subset of a group of nodes $\{g\}$ as well as an additional node $v_j \notin \{g\}$, v_i would be affected by the subset and $v_j \notin \{g\}$ simultaneously. For example, if the signals observed at v_i are similar to the signals at $\{g\}$, the embedding of v_i is still close to those of $\{g\}$. However, if the signals of v_i are close to that of v_j, or the weight of $e(i, j)$ is significantly high, v_i will be far away from $\{g\}$ in the embedding space.

Such intuition of the embedding distribution can be used to find potentially low-quality nodes, which we analyze next. Figure 3b shows that a node v_{25} is affected by its neighboring green nodes and v_4 that is not included in the cluster (green dots). The red dot v_{22} is connected with the green dots $(v_{19}, v_{20}, v_{21}, v_{23}, v_{25}, v_{29})$. Since these nodes have similar spatial features and are connected, the nodes are expected to have similar observations. At $t = 0$, the distribution of the nodes seems like a cluster. However, v_{25} is far away from other green nodes and the red node at $t = 4$. There are two possible reasons. First, observations of v_{25} at $t = 4$ may be too different with those of other green nodes and the red node. Second, observations at v_4, which is only connected to v_{25} (not to other green nodes and the red node), might be too noisy. The first case violates our assumption (See Section 2.2, such that the observation at v_{25} should be similar to those of other green nodes.); therefore, the observations of v_{25} at $t = 4$ might be noisy or not reliable. In the second case, the observations of v_4 at $t = 4$ might be noisy. Thus, v_{25} and v_4 are candidates of low-quality nodes.

5.3 Data quality analysis

Since we do not have explicit labels for the data quality levels, it is not straightforward to directly evaluate the data quality inferred from DQ-LSTM. Instead, we can verify the inferred data quality by studying high and low quality examples from embedding distributions and associated meterological

observations. Table 2 shows meterological observations associated with the previously discussed embedding distribution at $t = 4$ (Figure 3b). The values $\mathbf{x}_{25}$ at v_{25} are the same as $\mathbf{x}_{20}, \mathbf{x}_{21}$, and $\mathbf{x}_{23}$; however, $\mathbf{x}_{25}$ is quite different than $\mathbf{x}_{19}, \mathbf{x}_{22}$, and $\mathbf{x}_{29}$. Moreover, the edge weights between v_{25} and other green nodes are not as large as weights between other green nodes. (v_{25} is much closer to the ocean than other green nodes.) As a result, it is not easy for v_{25} to be close to the green nodes (v_{20}, v_{21}, and v_{23} pull v_{25} and v_{19}, v_{22}, and v_{29} push v_{25}). On the other hand, since $\mathbf{x}_{25}$ is similar to $\mathbf{x}_4$ and $W_{25,4}$ is large, v_{25} is more likely to be close to v_4 as in Figure 3b.

Table 2: Observations and inferred DQL

	Temp	Press	Humid	DQL
4	28.4	1013.1	57.7	0.022
19	34.5	1012.2	35.8	0.038
20	28.1	1011.5	58.7	0.039
21	28.1	1011.5	58.7	0.039
22	38.1	1006.2	32.8	0.039
23	28.1	1011.5	58.7	0.038
25	28.1	1011.5	58.7	0.030
29	35.3	1014.3	40.0	0.039

Note that v_4 has very different geological features compared to the features of the green nodes and thus, v_4 is not connected to v_{22} or other green nodes except v_{25}. Consequently, v_{25} is the bridge node between v_4 and the cluster of v_{22}. Since a bridge node is affected by two (or more) different groups of nodes simultaneously, the quality level at the bridge node is more susceptible than those of other nodes. However, this does not directly mean that a bridge node must have a lower data quality level.

As Table 2 shows, s_4 has the lowest data quality level, which comes from the discrepancy between its neighboring signals and $\mathbf{x}_4$. Since v_4 is connected to v_{25}, v_4 pulls v_{25} and s_4, lowering s_{25} relative to data quality levels of the other green nodes that are correctly inferred.

6 Conclusion

In this work, we proposed our model, DQ-LSTM, which enables the automatic inference of data quality for spatiotemporal data. While existing works have modeled spatiotemporal data by assuming that all signals are equally reliable over time, we argue that it is important to differentiate data quality because the signals come from heterogeneous sources. To address the issue, we proposed our formulation of data quality levels that are assigned to different sources and inferred from a given dataset. We evaluate our concept of data quality by comparing DQ-LSTM to baselines in real-world climate forecasting tasks.

Acknowledgments

This work is supported in part by NSF Research Grant IIS-1254206 and IIS-1539608. The views and conclusions are those of the authors and should not be interpreted as representing the official policies of the funding agency, or the U.S. Government. We thank Michael Tsang for discussion and his comments that greatly improved the manuscript.

References

Mikhail Belkin and Partha Niyogi. Laplacian eigenmaps and spectral techniques for embedding and clustering. In *Advances in neural information processing systems*, pp. 585–591, 2002.

Joan Bruna, Wojciech Zaremba, Arthur Szlam, and Yann LeCun. Spectral networks and locally connected networks on graphs. In *Proceedings of the International Conference on Learning Representations (ICLR)*, 2014.

Siheng Chen, Aliaksei Sandryhaila, José MF Moura, and Jelena Kovacevic. Signal denoising on graphs via graph filtering. In *Signal and Information Processing (GlobalSIP), 2014 IEEE Global Conference on*, pp. 872–876. IEEE, 2014.

Fan RK Chung. *Spectral graph theory*. Number 92. American Mathematical Soc., 1997.

Michaël Defferrard, Xavier Bresson, and Pierre Vandergheynst. Convolutional neural networks on graphs with fast localized spectral filtering. In *Advances in Neural Information Processing Systems*, pp. 3844–3852, 2016.

Ian J Goodfellow, Jonathon Shlens, and Christian Szegedy. Explaining and harnessing adversarial examples. *arXiv preprint arXiv:1412.6572*, 2014.

Aditya Grover and Jure Leskovec. node2vec: Scalable feature learning for networks. In *Proceedings of the 22nd ACM SIGKDD international conference on Knowledge discovery and data mining*, pp. 855–864. ACM, 2016.

David K Hammond, Pierre Vandergheynst, and Rémi Gribonval. Wavelets on graphs via spectral graph theory. *Applied and Computational Harmonic Analysis*, 30(2):129–150, 2011.

Mikael Henaff, Joan Bruna, and Yann LeCun. Deep convolutional networks on graph-structured data. *arXiv preprint arXiv:1506.05163*, 2015.

Sepp Hochreiter and Jürgen Schmidhuber. Long short-term memory. *Neural computation*, 9(8):1735–1780, 1997.

Joseph Juran and A Blanton Godfrey. Quality handbook. *Republished McGraw-Hill*, pp. 173–178, 1999.

Diederik Kingma and Jimmy Ba. Adam: A method for stochastic optimization. In *Proceedings of the International Conference on Learning Representations (ICLR)*, 2015.

Thomas N Kipf and Max Welling. Semi-supervised classification with graph convolutional networks. In *Proceedings of the International Conference on Learning Representations (ICLR)*, 2017.

Pang Wei Koh and Percy Liang. Understanding black-box predictions via influence functions. *International Conference on Machine Learning*, 2017.

Alex Krizhevsky, Ilya Sutskever, and Geoffrey E Hinton. Imagenet classification with deep convolutional neural networks. In *Advances in neural information processing systems*, pp. 1097–1105, 2012.

Yaguang Li, Rose Yu, Cyrus Shahabi, and Yan Liu. Graph convolutional recurrent neural network: Data-driven traffic forecasting. *arXiv preprint arXiv:1707.01926*, 2017.

Laurens van der Maaten and Geoffrey Hinton. Visualizing data using t-sne. *Journal of Machine Learning Research*, 9(Nov):2579–2605, 2008.

Jonathan Mei and José MF Moura. Signal processing on graphs: Estimating the structure of a graph. In *Acoustics, Speech and Signal Processing (ICASSP), 2015 IEEE International Conference on*, pp. 5495–5499. IEEE, 2015.

Ali Yener Mutlu, Edward Bernat, and Selin Aviyente. A signal-processing-based approach to time-varying graph analysis for dynamic brain network identification. *Computational and mathematical methods in medicine*, 2012, 2012.

Thomas C Redman. *Data driven: profiting from your most important business asset*. Harvard Business Press, 2008.

Aliaksei Sandryhaila and José MF Moura. Discrete signal processing on graphs. *IEEE transactions on signal processing*, 61(7):1644–1656, 2013.

Xuesong Shi, Hui Feng, Muyuan Zhai, Tao Yang, and Bo Hu. Infinite impulse response graph filters in wireless sensor networks. *IEEE Signal Processing Letters*, 22(8):1113–1117, 2015.

Shuang Song, Kamalika Chaudhuri, and Anand Sarwate. Learning from data with heterogeneous noise using sgd. In *Artificial Intelligence and Statistics*, pp. 894–902, 2015.

Ruth Urner, Shai Ben David, and Ohad Shamir. Learning from weak teachers. In *Artificial Intelligence and Statistics*, pp. 1252–1260, 2012.

Ulrike Von Luxburg. A tutorial on spectral clustering. *Statistics and computing*, 17(4):395–416, 2007.

Bing Yu, Haoteng Yin, and Zhanxing Zhu. Spatio-temporal graph convolutional neural network: A deep learning framework for traffic forecasting. *arXiv preprint arXiv:1709.04875*, 2017.

Qingbao Yu, Erik B Erhardt, Jing Sui, Yuhui Du, Hao He, Devon Hjelm, Mustafa S Cetin, Srinivas Rachakonda, Robyn L Miller, Godfrey Pearlson, et al. Assessing dynamic brain graphs of time-varying connectivity in fmri data: application to healthy controls and patients with schizophrenia. *Neuroimage*, 107:345–355, 2015.

Chicheng Zhang and Kamalika Chaudhuri. Active learning from weak and strong labelers. In *Advances in Neural Information Processing Systems*, pp. 703–711, 2015.

Dengyong Zhou and Bernhard Schölkopf. A regularization framework for learning from graph data. In *ICML workshop on statistical relational learning and Its connections to other fields*, volume 15, pp. 67–68, 2004.

Xiaofan Zhu and Michael Rabbat. Graph spectral compressed sensing for sensor networks. In *Acoustics, Speech and Signal Processing (ICASSP), 2012 IEEE International Conference on*, pp. 2865–2868. IEEE, 2012.

A DATASET

In order to have a fair comparison, we use real-world meteorological measurements from two commercial weather service providing real-time weather information, *Weather Underground*(WU)[1] and *WeatherBug*(WB)[2]. Both services use observations from automated personal weather stations (PWS). The PWS are illustrated in Figure 4.

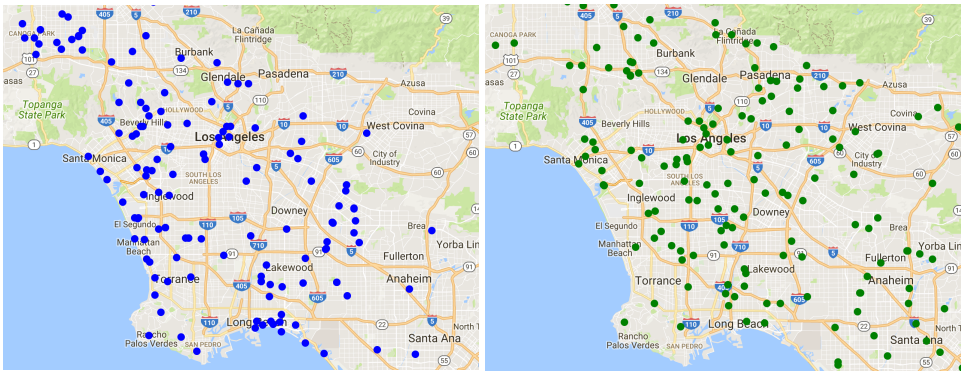

(a) Weather Underground (b) WeatherBug

Figure 4: Personal weather stations distributed over Los Angeles area

In the dataset, each station is distributed around Los Angeles County and land characteristics where the station is located at are provided. These characteristics would be used as a set of input features, $\mathbf{V}_i$. The list of the static characteristics is:

Table 3: Land features

Name	Unit	Description
Latitude	degree (°)	An angle which ranges from 0 at the Equator to 90 at the poles
Longitude	degree (°)	An angule which ranges from 0 at the Prime Meridian to +180 eastward and 180 westward
Elevation	ft	Elevation from average sea level
Tree fraction	dimensionless	Fraction covered by tree in that neighborhood
Vegetation fraction	dimensionless	Fraction of the neighborhood covered by vegetation
Albedo	dimensionless	Reflected amount of incoming shortwave
Distance from coast	m	Distance from the nearest coastal point
Impervious fraction	dimensionless	Fraction of the neighborhood covered by impervious material
Canopy width	ft	Width of the buildings to the centerline of streets
Building height	ft	Average height of buildings in neighborhood
Canopy direction	degree (°)	The direction of the canopy in degrees from 0-90

At each station, a number of weather data are observed through the installed instruments and recorded. The types of measurements are *Temperature, Pressure, Relative humidity, Solar radiation, Precipitation, Wind speed*, and *Wind direction*.

Table 4: Meteorological observations

	Temperature	Pressure	Relative Humidity	Solar Radiation	Precipitation	Wind Speed	Wind Direction
Unit	°C	mbar	%	W/m^2	mm	km/h	degree

[1]https://www.wunderground.com/
[2]http://weather.weatherbug.com/